University of Alberta

Light Curves of Very Compact Neutron Stars

by

Scott Olausen 

A thesis submitted to the Faculty of Graduate Studies and Research in partial fulfillment of the requirements for the degree of Master of Science

Department of Physics

Edmonton, Alberta
Fall 2008

Your file Votre référence
ISBN: 978-0-494-47380-1
Our file Notre référence
ISBN: 978-0-494-47380-1

University of Alberta

Library Release Form

NAME OF AUTHOR:	Scott Olausen
TITLE OF THESIS:	Light Curves of Very Compact Neutron Stars
DEGREE:	Master of Science
YEAR THIS DEGREE GRANTED:	2008

Scott Olausen
10939-72 Avenue
Edmonton, Alberta
T6G 0B1

September 10, 2008
26

University of Alberta

Faculty of Graduate Studies and Research

The undersigned certify that they have read, and recommend to the Faculty of Graduate Studies and Research for acceptance, a thesis entitled **Light Curves of Very Compact Neutron Stars** submitted by **Scott Olausen** in partial fulfillment of the requirements for the degree of Master of Science.

Sharon Morsink (Supervisor)

Valeri Frolov (Chair)

Suneeta Vardarajan (External)

Craig Heinke

DATE: _____

Abstract

Neutron stars are some of the densest and most compact objects in the universe with gravity so powerful that the light they emit can be bent around themselves to make more of their surface visible than would otherwise be possible. The very compact neutron stars that this work investigates can be subdivided into two categories. What we term *highly compact* neutron stars satisfy $R/M < 3.52$ and their entire surface is visible to a distant observer. *Ultracompact* neutron stars, with $R/M < 3$, have such intense gravity that some of the light that they emit cannot escape and instead falls back onto their surface. On all of these stars there are regions that can be multiply imaged, where two photons are emitted from the same point in different directions and both reach the same observer. The added computational difficulty that occurs when dealing with multiple images has limited previous investigation of these stars and their light curves. We develop a procedure for calculating the light curves produced by hot spots on very compact neutron stars that can account for multiple images. With this method in place we calculate light curves for many models of very compact stars and present how their shape and features are affected by the size and spin of the star, and the properties of the emitting spot.

Contents

List of Figures

Chapter 1

Introduction

Neutron stars, together with white dwarf stars and black holes, comprise the end products of stellar evolution; all stars will eventually end up as one of these astronomical objects. As low mass stars (those with main sequence mass of $M \lesssim 8M_{\odot}$) reach the end of their lives, their cores become white dwarf stars, composed chiefly of carbon and oxygen and supported from further collapse by electron degeneracy pressure, while their outer layers are gently shed in the form of a planetary nebula. Conversely, higher mass stars develop iron cores with masses greater than the Chandrasekhar limit of $M \approx 1.4M_{\odot}$ beyond which electron degeneracy pressure cannot prevent further collapse. As the core continues to collapse it becomes so dense that the process of inverse beta decay

$$e^{-} + p \rightarrow n + \nu$$

takes place, converting most of the matter in the core into neutrons [22], which continues to collapse until it is finally halted by neutron degeneracy pressure. The collision of the still-collapsing outer layers of the star with this newly formed hard surface causes a type II supernova which leaves behind only the newly formed neutron star. For extremely high mass stars ($M \gtrsim 25M_{\odot}$) their iron cores are too massive even for neutron degeneracy pressure to support them; nothing can stop their collapse into a black hole.

Neutron stars have a radius on the order of 10 km, and considering that a typical neutron star mass is $\sim 1.4M_{\odot}$, it is no surprise to find that with densities of $\sim 10^{15}\,\mathrm{g/cm^3}$, on par with atomic nuclei, they are the densest, most compact objects in the universe short of a black hole. Not only that, but during the collapse of a core conservation of angular momentum causes its rotation speed to greatly increase, so young neutron stars typically spin with frequencies on the order of 10-50 Hz. Core collapse also boosts enormously the magnetic fields of neutron stars in a similar manner, and the rotation

of the strong magnetic field results in a loss of energy that slows the star down. This phenomenon is known as magnetic braking, and because of it older neutron stars can have rotation periods of up to several seconds. Older neutron stars in binary systems, however, can undergo recycling, wherein they are spun back up to even greater rotation speeds by accreting material from their companion star, leading to rotation rates of hundreds of times per second. The highest confirmed rotation rate for a neutron star currently stands at 716 Hz [9].

Because they are so tiny and are no longer undergoing nuclear reactions, neutron stars are among the dimmest objects in the universe. Nevertheless, they can be visible by means other than thermal emission. A neutron star whose magnetic axis is not aligned with its spin axis will emit light in a narrow beam that is aligned with its magnetic poles. If this beam crosses our line of sight, we will see the star as a radio pulsar. Another way neutron stars can become visible is by accreting matter from a companion star as mentioned above. As the matter falls onto the star it heats up to temperatures of about 10^7 K which can be observed in the X-ray spectrum; such stars are called X-ray binaries. X-ray binaries with high mass donor stars (HMXBs) usually have high enough magnetic fields that accreting matter is funneled into the magnetic poles, revealing themselves as X-ray pulsars. Those with low mass donor stars (LMXBs) generally do not have high enough magnetic fields to produce pulsations; instead they can undergo X-ray bursts, caused by thermonuclear explosions in layers of matter accreted onto the star [2]. There is, however, also a small class of about 10 LMXBs known as accretion powered X-ray pulsars that exhibit both thermonuclear X-ray bursts as well as occasional coherent pulsations, first discovered with the observation of pulsations in the LMXB SAX J1808 in 1998 [23].

The extreme densities of neutron star matter mean that we cannot create comparable matter in the lab to study, so our knowledge of its properties and equation of state is limited. In addition, since models of neutron star structure and behaviour depend closely on the equation of state, our knowledge of neutron stars themselves is thus limited as well. There are many different theories and models, but investigation and testing is restricted to what information we can get from observations of neutron stars and neutron star phenomena. For example, the extremely high rotation speeds that are observed for some neutron stars can be used to restrict their possible maximum size to what is known as the Keplerian or mass-shed limit. This limit is reached when the star is rotating so fast that material does not remain gravitationally bound to its surface; it depends on the equation of state as well as the mass and radius of the star [5], but a good approximation exists that is independent of the equation of state [11]. Unfortunately the present limits

found by this particular method don't yet provide useful constraints on the equation of state.

In this work we are not concerned with rapidly rotating stars, however; instead we deal with very small, compact stars. Specifically, the very compact objects that we consider are those which fall into one of two groups, which we call *highly compact* and *ultracompact*. The gravity of a highly compact object is so strong that due to the extreme light bending its entire surface is visible to an observer at infinity. As a consequence, there exist points on the object from which two or more photons may be emitted in different directions and each reach the same observer; that is, parts of the object produce multiple visible images. Ultracompact objects, on the other hand, experience such powerful gravity that not all light emitted from the object can even escape to infinity; instead some of it falls back to the object's surface (if *no* light can escape from the object, then we of course have a black hole). In particular, given units of $c = G = 1$, neutron stars with $\frac{R}{M} < 3.52$ exhibit the behaviour of highly compact objects, and those with $\frac{R}{M} < 3$ are ultracompact (we will derive these numbers in Chapter 2).

As mentioned above, neutron stars are among the most compact objects in the universe, yet it is not known whether some or even any of them can fall in the realm of highly compact or ultracompact objects. Although the mass of neutron stars is often easy to determine, especially for those in binary systems, it is almost impossible to deduce their radius from present observations. Many neutron star models and equations of state predict radii that exclude ultracompact configurations in particular, but since precise limitations on neutron star masses and equations of state are not yet known this is hardly definitive. Indeed, there is a small amount of literature that has investigated and found stable configurations for ultracompact neutron stars with certain equations of state [10, 15].

The purpose of this research is to examine some of the observable effects of highly compact and ultracompact neutron stars by investigating the light curves produced by hot spots on such stars. The pioneering work in this area was done by Pechenick et al. and Ftaclas et al. [17, 6], who were the first to derive a method of including strong gravity and light bending in neutron star light curves; they even calculated light curves for a couple of highly compact neutron stars. Nemiroff et al. [16] continued with an examination of light curves produced by ultracompact stars in a few simple configurations. They also looked at changes to the Eddington luminosity of an ultracompact star as well as the possibilty of gravitationally bound neutrino orbits. Our goal is a more detailed examination of their light curves: what distinguishing features they have and under what circumstances they are or are not observable.

This work is organized in a straightforward manner as follows. In Chapter 2 we develop the theory and method for calculating light curves for highly compact and ultra-compact neutron stars. Section 2.1 provides an overview of the Schwarzschild geometry and how light travels through it. Section 2.2 describes the procedure for calculating neutron star light curves and modifies it to account for when multiple images are visible. One of the computational difficulties that was encountered is tackled in Section 2.3. We also determine some important constraints on neutron star compactness in Section 2.4. Chapter 3 presents the light curves we produced. Sections 3.1 through 3.5 present the changes to the light curves that result from varying different parameters. In Section 3.6 we discuss whether it is possible for a light curve from a highly compact or ultracompact star to match observed data by looking at pulsations from the neutron star SAX J1808. Finally, Chapter 4 contains the final summary and conclusion.

Chapter 2

Theory

The aim of this chapter is to construct a procedure to calculate light curves from neutron stars, particularly from highly compact and ultracompact ones. Before we can do that, however, we must also develop the necessary theory.

We need to know the spacetime metric that photons travel through as they travel from the star to the observer. We begin by assuming that the star, and consequently the overall spacetime, is spherically symmetric, which simplifies matters greatly. The metric for the star's interior, then, is given by a spherically symmetric metric described by MTW [14] that depends on the star's equation of state. For our purposes the details of this metric are unimportant, because we are interested only in the motion of photons after they have left the star's surface and are in the region exterior to it. The only two things we need to know about the star are its mass and radius. Because we are assuming spherical symmetry, Birkhoff's theorem guarantees that the external metric is given by the Schwarzschild metric and characterized only by the star's mass [14].

2.1 Photon Orbits in the Schwarzschild Metric

Given a spherically symmetric star with mass M the region external to it is described by the Schwarzschild metric:

$$\mathrm{d}s^2 = -\left(1 - \frac{2GM}{c^2 r}\right)(c\,\mathrm{d}t)^2 + \left(1 - \frac{2GM}{c^2 r}\right)^{-1}\mathrm{d}r^2 + r^2\mathrm{d}\theta^2 + r^2\sin^2\theta\,\mathrm{d}\phi^2, \qquad (2.1)$$

which in units of $c = G = 1$ becomes

$$\mathrm{d}s^2 = -(1 - 2M/r)\mathrm{d}t^2 + (1 - 2M/r)^{-1}\mathrm{d}r^2 + r^2\mathrm{d}\theta^2 + r^2\sin^2\theta\,\mathrm{d}\phi^2. \qquad (2.2)$$

Photons move along null geodesics. Because the Schwarzschild metric is independent of t and ϕ, we know that the following quantities are conserved along photon paths:

$$e = -\xi \cdot u = (1 - 2M/r)\frac{\mathrm{d}t}{\mathrm{d}\lambda} \tag{2.3}$$

$$l = n \cdot u = r^2 \sin^2\theta \frac{\mathrm{d}\phi}{\mathrm{d}\lambda} \tag{2.4}$$

where u is the photon's four-velocity, ξ and n are respectively the time-like and rotational Killing vectors of the metric, and λ is an affine parameter. In addition, the quantities e and l can be interpreted as the photon's energy and angular momentum, respectively [8, 14]. Moreover, since photons follow null geodesics, the tangent vector must be null:

$$u \cdot u = -(1 - 2M/r)\left(\frac{\mathrm{d}t}{\mathrm{d}\lambda}\right)^2 + (1 - 2M/r)^{-1}\left(\frac{\mathrm{d}r}{\mathrm{d}\lambda}\right)^2 + r^2\left(\frac{\mathrm{d}\theta}{\mathrm{d}\lambda}\right)^2 + r^2\sin^2\theta\left(\frac{\mathrm{d}\phi}{\mathrm{d}\lambda}\right)^2 = 0 \tag{2.5}$$

The spherical symmetry of the metric allows us to, without loss of generality, take any photon orbit to be in the plane of the equator, $\theta = \pi/2$, which gives us

$$-(1 - 2M/r)\left(\frac{\mathrm{d}t}{\mathrm{d}\lambda}\right)^2 + (1 - 2M/r)^{-1}\left(\frac{\mathrm{d}r}{\mathrm{d}\lambda}\right)^2 + r^2\left(\frac{\mathrm{d}\phi}{\mathrm{d}\lambda}\right)^2 = 0 \tag{2.6}$$

Using equations 2.3 and 2.4 to eliminate $dt/d\lambda$ and $d\phi/d\lambda$ from the above equation gives the formula

$$-(1 - 2M/r)^{-1}e^2 + (1 - 2M/r)^{-1}\left(\frac{\mathrm{d}r}{\mathrm{d}\lambda}\right)^2 + \frac{l^2}{r^2} = 0 \tag{2.7}$$

To calculate the shape of photon orbits, however, we want to find $d\phi/dr$. Solve equation 2.7 for $dr/d\lambda$, then solve equation 2.4 for $d\phi/d\lambda$ and divide the first result into the second to get

$$\frac{\mathrm{d}\phi}{\mathrm{d}r} = \frac{1}{r^2}\left[\frac{e^2}{l^2} - \frac{(1 - 2M/r)}{r^2}\right]^{-1/2} = \frac{1}{r^2}\left[b^{-2} - B^{-2}(r)\right]^{-1/2} \tag{2.8}$$

where $b = l/e$ is the impact parameter of the photon orbit, and

$$B^{-2}(r) = \frac{(1 - 2M/r)}{r^2} \tag{2.9}$$

is the effective potential for photon orbits (following the definition given in MTW [14]).

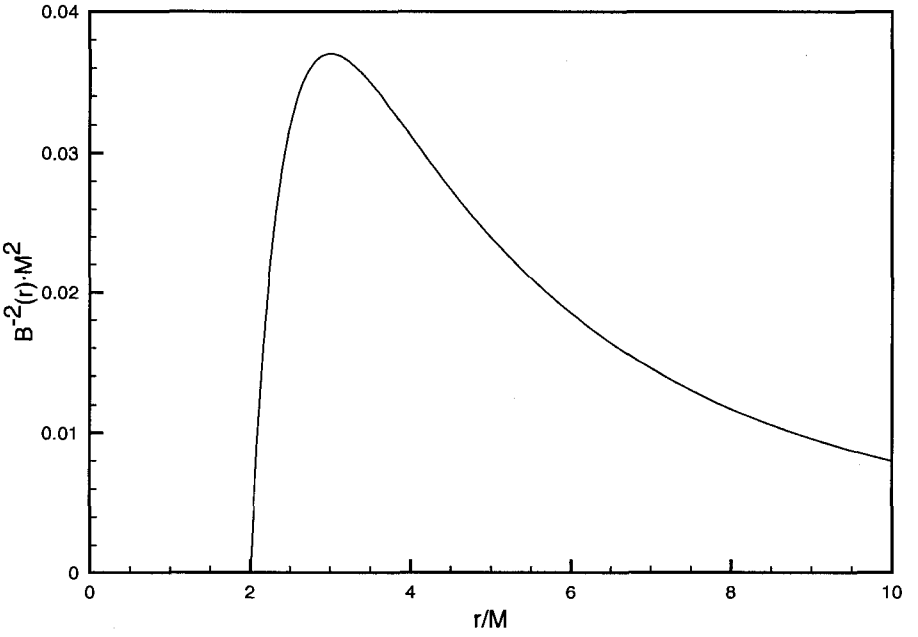

Figure 2.1: The effective potential for photon orbits, $B^{-2}(r)$.

2.1.1 The Photon Sphere

If we examine the effective potential curve $B^{-2}(r)$ for photon orbits, we see that there is a maximum of $B_{\max}^{-2} = \frac{1}{27M^2}$ at $r = 3M$. This means that photons are able to travel in circular orbits of radius $r = 3M$, a distance also known as the photon sphere. These orbits are unstable, however, and a small perturbation will cause them to spiral into or away from the center of attraction [8].

The shape of the potential also means that light rays emitted outward from a surface located at $R < 3M$ will not necessarily escape to infinity. Since the quantity $\frac{d\phi}{dr}$ from equation 2.8 must be real, it follows that only photons whose impact parameter satisfies $b^{-2} > B_{\max}^{-2}$ will escape; other light rays will only travel outward a short distance before falling back to the surface.

Suppose a photon is emitted outward from a surface $r = R$ in the Schwarzschild spacetime. An observer at rest measures the angle of emission α relative to the radial direction (see Figure 2.2) in his orthonormal frame by

$$\sin\alpha = \frac{u \cdot e_{\hat{\phi}}}{u \cdot e_{\hat{t}}} \tag{2.10}$$

where u is the photon's four-velocity, $e_{\hat{t}}$ is the observer's four-velocity, and $e_{\hat{r}}$, $e_{\hat{\theta}}$, and $e_{\hat{\phi}}$

are the additional three orthonormal basis vectors describing his frame [8, 14]. Solving this gives us

$$\sin\alpha = \frac{b\sqrt{1-2M/R}}{R} = \frac{b}{B(R)}. \tag{2.11}$$

For this photon to escape a star with surface $R < 3M$ it must satisfy $b < 3\sqrt{3}M$, so by substituting this value into equation 2.11 we can find the critical angle of emission α_{crit} beyond which light rays will not escape to infinity:

$$\sin\alpha_{\text{crit}} = \frac{3\sqrt{3}M\sqrt{1-2M/R}}{R}. \tag{2.12}$$

Only light rays emitted at an angle $\alpha < \alpha_{\text{crit}}$ will escape to infinity and be observable.

2.1.2 Light Bending

Suppose we have a spherical neutron star with surface located at $r = R$, where $R > 2M$. A light ray is emitted from a spot on the star at an angle α measured with respect to the radial direction such that it reaches an observer at infinity. From equation 2.11, we can find the impact parameter of the light ray,

$$b = \frac{R\sin\alpha}{\sqrt{1-2M/R}}, \tag{2.13}$$

and use it to calculate the angular separation between the point of emission and the observer, also known as the light bending. To calculate this value we integrate equation 2.8 over the photon's path from R to infinity:

$$\psi = \int_R^\infty \mathrm{d}r \frac{b}{r^2}\left[1 - \frac{b^2}{r^2}\left(1 - \frac{2M}{r}\right)\right]^{-1/2}. \tag{2.14}$$

Equation 2.14 cannot be solved analytically, but Belobodorov derived a simple formula, $1-\cos\psi = (1-\cos\alpha)(1-r/2M)^{-1}$, that provides a good approximation to the integral for $R \geq 4M$ [1]. We, however, are interested in more compact stars and so must compute the integral numerically.

From equation 2.14 we can perform a change of variables by defining $u = R/r$ and $du = -Rdr/r^2$ and the substitution $\hat{b} = b/R$, we get

$$\psi = \int_0^1 \mathrm{d}u\,\hat{b}\left[1 - \hat{b}^2u^2\left(1 - \frac{2Mu}{R}\right)\right]^{-1/2}, \tag{2.15}$$

which is an elliptic integral. Note that in flat spacetime ($M/R = 0$), we get the expected result of $\psi = \alpha$. The maximum value of ψ occurs when the impact parameter is maximal, which in turn can be determined by setting $\alpha = \pi/2$ if the photon is emitted from outside the photon sphere, and by setting $\alpha = \alpha_{\text{crit}}$ from equation 2.12 otherwise. Doing this gives us:

$$b_{\max} = \begin{cases} \frac{R}{\sqrt{1-2M/R}} & R > 3M \\ 3\sqrt{3}M & R \leq 3M \end{cases} \tag{2.16}$$

$$\psi_{\max} = \begin{cases} \int_0^1 \mathrm{d}u \left[\left(1 - \frac{2M}{R}\right) - u^2\left(1 - \frac{2Mu}{R}\right)\right]^{-1/2} & R > 3M \\ \int_0^1 \mathrm{d}u \left[\frac{R^2}{27M^2} - u^2\left(1 - \frac{2Mu}{R}\right)\right]^{-1/2} & R \leq 3M \end{cases}, \tag{2.17}$$

which is graphed in Figure 2.3(the shading is explained below). Notice that for $R > 3M$, $\psi_{\max}$ is finite and increases as R/M decreases, whereas for $R \leq 3M$ the integral diverges and $\psi_{\max} = \infty$. Physically, this means that a photon emitted from a surface at $R \leq 3M$ can be bent through an arbitrarily large angle (circle around the center of mass an arbitrary number of times) by being emitted at an angle arbitrarily close to the critical angle α_{crit} defined in equation 2.12.

2.2 Calculating the Light Curve

With the relevant theory in place we may now develop a procedure to calculate the light curve.

The geometry of this problem is shown in Figure 2.2. We consider a star with radius R and mass M that rotates with period P around a spin axis inclined at an angle i, called the inclination angle, to the observer. The star has on it an emitting spot located at colatitude θ and azimuthal angle $\phi = \omega t$ (note that these angles are not the same as the Schwarzschild coordinates θ and ϕ defined in Section 2.1). We now define a coordinate system where the z-axis points along the spin axis of the star and the x-axis points along the azimuthal angle $\phi = 0$ in the equatorial plane of the star. In this coordinate system we identify the unit vectors $\mathbf{k}$ and $\mathbf{n}$, which originate at the emitting spot and point to the observer and along the normal to the surface, respectively. We also identify the unit vector $\boldsymbol{\beta}$ that points along the direction of motion of the spot due to the star's rotation.

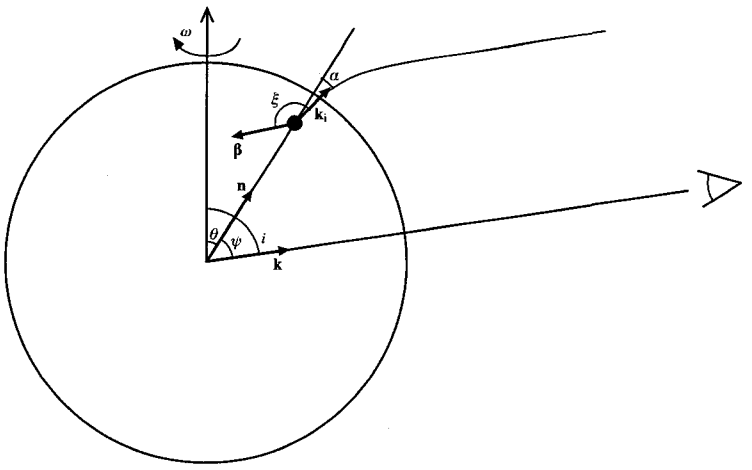

Figure 2.2: Geometry for calculating light curves. A photon is emitted from the star in direction $\mathbf{k_i}$ which forms an angle α with the normal to the star's surface. When it reaches the distant observer it is now travelling in direction $\mathbf{k}$ which forms an angle ψ with the normal to the star's surface. θ is the angle between the point of emission on the star and its spin axis, while i is the angle between the observer and the spin axis of the star. Finally, ξ is the angle between the direction of photon emission and the direction of the star's rotation. Note that vectors $\mathbf{k}$ and $\mathbf{n}$ are drawn at the center of the star to avoid crowding the diagram, although they are defined as originating from the point of emission.

The components of these vectors are

$$\mathbf{k} = (\sin i, 0, \cos i) \tag{2.18}$$

$$\mathbf{n} = (\sin\theta\cos\phi, \sin\theta\sin\phi, \cos\theta) \tag{2.19}$$

$$\boldsymbol{\beta} = (-\sin\phi, \cos\phi, 0). \tag{2.20}$$

In the observer's frame, photons are emitted from the spot at an angle α with respect to the radial direction, and reach the observer after being bent through an angle ψ, with

$$\cos\psi = \mathbf{k}\cdot\mathbf{n} = \cos\theta\cos i + \sin\theta\sin i\cos\phi. \tag{2.21}$$

Let $\mathbf{k_i}$ be the unit vector pointing in the initial direction of photon emission. Because photon orbits in the Schwarzschild metric are planar, we can obtain the components of

$\mathbf{k}_\mathrm{i}$ by solving the system of equations

$$\cos\alpha = \mathbf{k}_\mathrm{i}\cdot\mathbf{n} \tag{2.22}$$

$$\cos(\psi-\alpha) = \mathbf{k}_\mathrm{i}\cdot\mathbf{k} \tag{2.23}$$

$$0 = \det\left[\begin{array}{ccc}\mathbf{k} & \mathbf{n} & \mathbf{k}_\mathrm{i}\end{array}\right], \tag{2.24}$$

where the third equation follows from the linear dependence of $\mathbf{k}$, $\mathbf{n}$, and $\mathbf{k}_\mathrm{i}$. The result is

$$\mathbf{k}_\mathrm{i} = \left(\frac{\sin i\sin\alpha}{\sin\psi}+\frac{\sin\theta\cos\phi\sin(\psi-\alpha)}{\sin\psi}, \frac{\sin\theta\sin\phi\sin(\psi-\alpha)}{\sin\psi}, \frac{\cos i\sin\alpha}{\sin\psi}+\frac{\cos\theta\sin(\psi-\alpha)}{\sin\psi}\right). \tag{2.25}$$

From this result we can express ξ in terms of α, ψ, i, and ϕ:

$$\cos\xi = \mathbf{k}_\mathrm{i}\cdot\boldsymbol{\beta} = -\frac{\sin i\sin\alpha\sin\phi}{\sin\psi}. \tag{2.26}$$

In flat spacetime there is no light bending, so $\psi=\alpha$ and $\mathbf{k}_\mathrm{i}=\mathbf{k}$, but in the Schwarzschild metric the relation between α and ψ is given by equation 2.15:

$$\psi = \int_0^1 du\,\hat{b}\left[1-\hat{b}^2u^2\left(1-\frac{2Mu}{R}\right)\right]^{-1/2}, \tag{2.27}$$

where $\hat{b}=b/R$ for the impact parameter, b, given by

$$b = \frac{R\sin\alpha}{\sqrt{1-2M/R}}. \tag{2.28}$$

The flux received by the observer is given by $\mathrm{d}F_o = I_\mathrm{obs}\mathrm{d}\Omega/D^2$, where I_obs is the observed intensity, D is the distance between source and observer, and $\mathrm{d}\Omega$ is the solid angle of the image on the observer's sky. This angle is given by

$$\mathrm{d}\Omega = b\,\mathrm{d}b\,\mathrm{d}\varphi, \tag{2.29}$$

where b is the impact parameter and φ is an azimuthal angle corresponding to rotation about $\mathbf{k}$. Similarly, we can describe the area of the emitting spot on the surface of the star in the observer's frame using (ψ,φ) coordinates as

$$\mathrm{d}S = R^2\sin\psi\mathrm{d}\psi\mathrm{d}\varphi. \tag{2.30}$$

Using equations 2.28 and 2.30, then, equation 2.29 becomes

$$\begin{aligned} \mathrm{d}\Omega &= \frac{\mathrm{d}S\cos\alpha}{1-2M/R}\frac{\sin\alpha}{\sin\psi}\frac{\mathrm{d}\alpha}{\mathrm{d}\psi} \\ &= \frac{\mathrm{d}S\cos\alpha}{\sqrt{1-2M/R}}\frac{\sin\alpha}{\sin\psi\cos\alpha}\frac{1}{\mathrm{d}\psi/\mathrm{d}\hat{b}}, \end{aligned} \tag{2.31}$$

where

$$\frac{\mathrm{d}\psi}{\mathrm{d}\hat{b}} = \int_0^1 \mathrm{d}u \left[1-\hat{b}^2u^2\left(1-\frac{2Mu}{R}\right)\right]^{-3/2}. \tag{2.32}$$

2.2.1 Rotation

All of the above work applies precisely for a static, spherically symmetric neutron star, because as previously discussed Birkhoff's theorem requires the external metric to be Schwarzschild. Realistically, however, we expect all neutron stars to rotate; certainly any star that produces a light curve has to be rotating in order to do so. As a simple approximation for dealing with stellar rotation, we will merely bring in corrections from special relativity while continuing to work in the Schwarzschild metric. Strictly speaking, in order to account exactly for the star's rotation, we should be working in an appropriate axisymmetric rotating spacetime that incorporates the deformation of the star into an oblate spheroid [5]. For slowly rotating stars, however, we can neglect these effects as well as the differing times of flight between photons emitted from different locations on the star, and our approximation is sufficiently accurate [3, 4].

Let us thus consider the frame of emission, corotating with the star. In this frame, the emitting spot has an area of $\mathrm{d}S_{\mathrm{em}}$ and emits photons at an angle α_{em} to the normal, and these two quantities are related to their counterparts in the observer's frame by the result that the projection of the spot area onto a plane perpendicular to the direction of photon emission is Lorentz invariant [18]:

$$\mathrm{d}S\cos\alpha = \mathrm{d}S_{\mathrm{em}}\cos\alpha_{\mathrm{em}}. \tag{2.33}$$

We also relate the angles α and α_{em} by the relativistic aberration formula $\cos\alpha_{\mathrm{em}} = \eta\cos\alpha$ [20], where η is the Doppler factor. Then equation 2.31 becomes

$$\begin{aligned} \mathrm{d}\Omega &= \frac{\mathrm{d}S_{\mathrm{em}}\cos\alpha_{\mathrm{em}}}{\sqrt{1-2M/R}}\frac{\sin\alpha}{\sin\psi\cos\alpha}\frac{1}{\mathrm{d}\psi/\mathrm{d}\hat{b}} \\ &= \frac{\mathrm{d}S_{\mathrm{em}}\eta}{\sqrt{1-2M/R}}\frac{\sin\alpha}{\sin\psi}\frac{1}{\mathrm{d}\psi/\mathrm{d}\hat{b}}. \end{aligned} \tag{2.34}$$

The Doppler factor can be found by

$$\eta = \frac{\sqrt{1-\beta^2}}{1-\beta\cos\xi}, \tag{2.35}$$

where $\cos\xi$ comes from equation 2.26 and $\beta = v/c$ is the velocity of the spot measured in the nonrotating frame

$$\beta = \frac{2\pi R}{cP}\frac{\sin\theta}{\sqrt{1-2M/R}}. \tag{2.36}$$

Finally, the observed radiation intensity $I_{\rm obs}$ is related to the intensity of the emitted radiation $I_{\rm em}$ by the Lorentz invariant relation [14]

$$\frac{I_{\rm obs}}{\nu_{\rm obs}^3} = \frac{I_{\rm em}}{\nu_{\rm em}^3}, \tag{2.37}$$

which gives the result

$$\begin{aligned} I_{\rm obs} &= \left(\frac{\nu_{\rm obs}}{\nu_{\rm em}}\right)^3 I_{\rm em} \\ &= (1-2M/R)^{3/2}\eta^3 I_{\rm em}. \end{aligned} \tag{2.38}$$

If we account for the possibility that the radiation emitted by the spot depends on the angle of emission $\alpha_{\rm em}$, then we can express its intensity by $I_{\rm em} = I_0 f(\alpha_{\rm em})$ (for isotropic emission, $f(\alpha_{\rm em}) = 1$). This gives us our final expression for received flux from the emitting spot on the star as

$$\mathrm{d}F_o = \frac{\mathrm{d}S_{\rm em}}{D^2} I_0 f(\alpha_{\rm em})(1-2M/R)\eta^4 \frac{\sin\alpha}{\sin\psi}\frac{1}{\mathrm{d}\psi/\mathrm{d}\hat{b}}. \tag{2.39}$$

The standard procedure for calculating the flux from an emitting spot of finite size is as follows:

1. Select a rotation phase ϕ, and calculate the light bending angle ψ from equation 2.21.

2. Determine $\alpha(\psi)$ by inverting equation 2.27. One may do this numerically, or for stars of $R > 4M$ by using the polynomial relationship found by Beloborodov [1].

3. Calculate $\mathrm{d}\psi/\mathrm{d}\hat{b}$ from equation 2.32.

4. Calculate $\cos\xi$ from equation 2.26 and use it to determine the Doppler factor η. Use this to evaluate the visibility condition $\cos\alpha_{\rm em} > 0$.

5. Integrate equation 2.39 over the visible area of the spot.

Note that this result is the monochromatic flux $F_o(\nu_o)$, which for simplicity's sake is what we will be calculating. Given an equation for $I_o(\nu_o)$ one may integrate $\int F_o(\nu_o)\mathrm{d}\nu_o$ to get the bolometric flux (this typically brings in an extra term of $\frac{\nu_{\mathrm{obs}}}{\nu_{\mathrm{em}}} = \sqrt{1-2M/R}\eta$), although actual observed light curves are usually only measured over a finite band of frequencies, so neither the monochromatic nor the bolometric flux are entirely appropriate.

2.2.2 Multiple Images

The procedure outlined in the previous section is adequate for large enough neutron stars where the light bending is not extreme, but we are considering highly compact and ultracompact stars. On such stars, there are locations where two or more light rays may be emitted from the same point in different directions, travel along separate orbits, and all reach the same observer. In order to determine for which stars we will encounter this phenomenon, we invert equation 2.17 to find the value of R/M for which $\psi_{\max}(R/M) > \pi$; this turns out to be $R < 3.52M$. In addition, we find that $\psi_{\max}(R/M) > 2\pi$ for $R < 3.02M$, meaning that all points on these stars produce multiple images (see Figure 2.3). In fact, for ultracompact stars, $\psi_{\max} = \infty$ and all points on the star produce an infinite number of images (which, fortunately, cover only a finite area in the sky and are therefore of finite brightness).

Since photons are propagated in a plane in Schwarzschild space, determining the light bending angles of all possible multiple images is straightforward. Equation 2.21 gives us the cosine of the light bending angle, so to get the light bending angles of all possible images, we merely take the (multi-valued) inverse cosine of this number. The angle of the primary image is equal to the primary value of the inverse cosine, while the other values give angles for other images. If we denote the angle of the primary image by ψ_0, we can express this explicitly:

$$\psi_n = \begin{cases} (n+1)\pi - \psi_0 & n \text{ odd} \\ n\pi + \psi_0 & n \text{ even} \end{cases}. \tag{2.40}$$

A version of the above procedure modified to account for multiple images is as follows:

1. For a star with given parameter R/M calculate $\psi_{\max}(R/M)$ from equation 2.17.

2. Select a rotation phase ϕ, and calculate the primary light bending angle ψ_0 from equation 2.21.

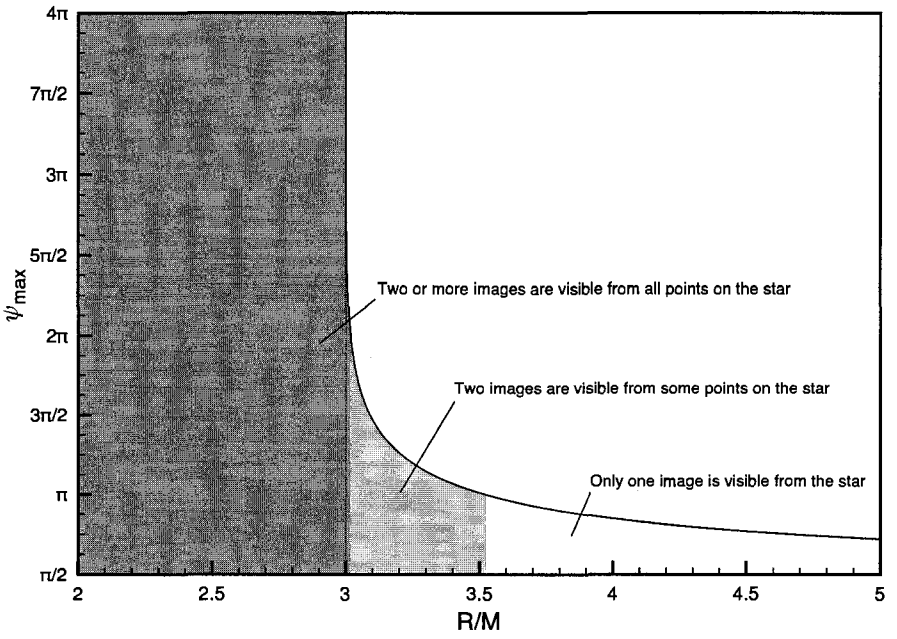

Figure 2.3: The maximum light bending angle for a star $\psi_{\max}$ as a function of its compactness R/M. For stars in the lighter shaded area ($R/M < 3.52$), some points on their surface produce two images visible to an observer at infinity. For stars in the darker shaded area ($R/M < 3.02$), all points on their surface produce at least two images. Note that $\psi_{\max} \to \infty$ for $R/M \leq 3$.

3. Determine whether and how many multiple images are present using equation 2.40 to find for what values of n $\psi_n < \psi_{\max}$.

4. Perform steps 2-4 from the previous procedure to calculate $\alpha_n(\psi_n)$, $\mathrm{d}\psi_n/\mathrm{d}\hat{b}$, and η_n for each image present. Note that the polynomial approximation for $\alpha_n(\psi_n)$ no longer holds for these stars and it must be found numerically. In the case of $\psi_{\max} = \infty$, the sequence may be truncated at $n = 2$ or 3, as the contribution from each image decreases rapidly as n increases.

5. To account for multiple images, then, equation 2.39 becomes

$$\mathrm{d}F_o = \frac{\mathrm{d}S_{\mathrm{em}}}{D^2} \sum_n I_0 f(\alpha_{\mathrm{em}})(1 - 2M/R)\eta_n^4 \frac{\sin\alpha_n}{\sin\psi_0} \frac{1}{\mathrm{d}\psi_n/\mathrm{d}\hat{b}}, \tag{2.41}$$

truncating the sum as before (We have $\sin\psi_0$ here instead of $\sin\psi_n$ because in our derivation $\sin\psi$ was defined only for $0 \leq \psi \leq \pi$). Integrate this equation over the spot area.

2.3 Numerical Computation of the Light Curve

The calculation of light curves was handled numerically, using computer code written in ANSI Standard C, and following the procedure for multiple images outlined above to calculate equation 2.41 over the area $\mathrm{d}S_{\mathrm{em}}$ of the emitting spot. Numerical integration was required at two points in the procedure, namely the calculation of $\alpha_n(\psi_n)$ for each image and the integration of equation 2.41 over the area of the emitting spot, and it was accomplished by means of the Romberg integration routines `qromb` and `qromo` from Press *et al.* [19]. To find $\alpha_n(\psi_n)$ we produce a table of values by calculating $\psi(\alpha)$ from equation 2.27 for many values of α from 0 to α_{crit}, and from that we are able to find α for any given value of ψ by way of an interpolation routine. In order to integrate equation 2.41 over the spot area, it is possible in general to set $\mathrm{d}S_{\mathrm{em}} = R^2 \sin\theta \mathrm{d}\theta\mathrm{d}\phi$, which gives us

$$F_o = \frac{R^2 I_0}{D^2}\mathcal{F}, \tag{2.42}$$

where $\mathcal{F}$ is the double integral in (θ, ϕ) coordinates

$$\mathcal{F} = \int\int \sum_n f(\alpha_{\mathrm{em}})(1 - 2M/R)\eta_n^4 \frac{\sin\alpha_n}{\sin\psi_0}\frac{1}{\mathrm{d}\psi_n/\mathrm{d}\hat{b}}\sin\theta \mathrm{d}\theta\mathrm{d}\phi, \tag{2.43}$$

with limits of integration in θ and ϕ defined by the size and shape of the spot. For stars that are compact enough to produce multiple images, however, this method runs into a problem: equation 2.34 for the solid angle subtended by the image in the observer's sky diverges at points on the star with $\sin\psi = 0$ but $\sin\alpha \neq 0$. At these points equation 2.43 is not integrable in (θ, ϕ) coordinates and so the integration routine fails. Fortunately, the behaviour of the function at these points is merely a coordinate singularity, and the problem disappears when we set $\mathrm{d}S_{\mathrm{em}} = R^2 \sin\psi \mathrm{d}\psi\mathrm{d}\varphi$. Here, $\sin\psi_0 = \sin\psi$, resulting in the double integral in (ψ, φ) coordinates

$$\mathcal{F} = \int\int \sum_n f(\alpha_{\mathrm{em}})(1 - 2M/R)\eta_n^4 \sin\alpha_n \frac{1}{\mathrm{d}\psi_n/\mathrm{d}\hat{b}}\mathrm{d}\psi\mathrm{d}\varphi. \tag{2.44}$$

Equation 2.44 contains no singularities and can be evaluated anywhere on the surface of a star. In theory, we could calculate the light curves everywhere over the star in (ψ, φ) coordinates, but in practice, except for regions near the points $\sin\psi = 0$, the integration routines converge much more slowly and less accurately for equation 2.44 than for equation 2.43. We therefore stuck to calculating equation 2.43 over the spot area if it contained no coordinate singularities. In cases where the spot area did contain

a coordinate singularity, a region roughly one degree in angular radius surrounding the singularity was calculated in (ψ, φ) coordinates, while the remainder of the spot area was evaluated in (θ, ϕ) coordinates.

2.4 Constraints on Neutron Star Compactness

At the beginning of this chapter we mentioned that the details of neutron stars' internal structure did not concern us, since we are only investigating the motion of photons in the region outside the star. To end the chapter, however, we will make a brief diversion into the subject where we will learn three important constraints on neutron star compactness.

There are several equations involved in determining the structure of a star, but the one we wish to examine is the Oppenheimer-Volkoff equation of hydrostatic equilibrium. This is the equation of hydrostatic equilibrium as applied to a spherically symmetric fluid in general relativity, and is given by

$$\frac{\mathrm{d}P}{\mathrm{d}r} = -\frac{(\rho + P)(m + 4\pi P r^3)}{r^2(1 - 2m/r)}, \tag{2.45}$$

where $P(r)$ is the star's internal pressure, $\rho(r)$ is its density, and $m(r)$ is the mass contained within radius r. For neutron stars, the equation of state of the fluid can be expressed in the equation $P(\rho)$ [22]. The surface of the star is defined as the radius R where pressure drops to zero, so that $P(R) = 0$ and $m(R) = M$ for the mass of the star M.

The first constraint comes from the $(1 - 2m/r)$ term in the denominator of equation 2.45. First we note that near the centre of the star $m(r) \propto r^3$, so $2m/r < 1$ there. Then we only need to see that as $2m/r \to 1$, the pressure gradient $\frac{\mathrm{d}P}{\mathrm{d}r} \to -\infty$, meaning that the pressure will drop to zero (at which point we have reached the surface of the star) well before this can happen. Since $m(R) = M$ we conclude that it is impossible for a static star to have radius $R \leq 2M$.

The second constraint, or the finite pressure limit, is found by solving equation 2.45 for a neutron star with constant density $\rho(r) = \rho_c$. When we examine the solution we find that the central pressure of such stars goes to infinity if they have radius $R \leq 2.25M$ [21]. Since a uniform density is the most compact form of density equation, and since physically possible neutron stars must have finite pressure, they must have $R > 2.25M$.

The third and strictest constraint on the compactness of a neutron star is the causality limit, which does not come from equation 2.45. Instead, it comes from imposing on the star's equation of state the causality condition that $\frac{\mathrm{d}P}{\mathrm{d}\rho} \leq c^2$, which means that the speed

of sound in the interior of the star should be below the speed of light c. Lindblom [13] calculated this limit assuming the star's equation of state was known for densities below some cutoff value ρ_0 and unknown at higher densities in the star's core, and he found that the limit depended on the star's mass M as well as ρ_0. These values for the causality limit ranged from $R = 2.8 \sim 2.85M$. In addition, Haensel et. al [7] found the causality limit for a neutron star with no crust to be $R = 2.83M$.

Chapter 3

Results

In this chapter we calculate and present light curves for many different configurations of highly compact and ultracompact stars. Our method follows the procedure outlined in the previous chapter to calculate the quantity $\mathcal{F}$ from equation 2.42 given a star of radius R and mass M rotating with period P about a spin axis aligned with the observer at angle i. We take the emitting spot on the star to be a spherical cap of angular diameter ρ centred at colatitude θ and azimuthal angle ϕ. In making the light curves the azimuthal angle ϕ also doubles as the rotation phase of the star, such that at $\phi = 0$ and $\phi = 2\pi$ the spot is facing the observer and at $\phi = \pi$ it is on the opposite side of the star. Finally, unless otherwise stated we assume isotropic emission ($f(\alpha_{\rm em}) = 1$ in equation 2.41, dropping the subscript from here on).

Since few realistic neutron star equations of state predict or are investigated to the high compactness that we are dealing with, we did not derive the radius and mass of our model stars from an equation of state. Instead we chose four values of R/M to investigate in detail: $R = 3.2M$ represents a highly compact star that is completely visible to the observer and produces multiple images; $R = 2.9M$ for an ultracompact star that still allows for a causal equation of state; $R = 2.3M$ for an ultracompact star just above the finite pressure (albeit well past the causal) limit for neutron star compactness; and $R = 2.6M$ for a star somewhere between the previous two (but also past the causal limit). Although we don't expect to find stars below the causal limit, we examine the properties of the latter two values of R/M anyway to get a better understanding of how extreme gravity affects the light curve. In addition, for all of these models we take as the star's mass the conventional choice of $M = 1.4M_{\odot}$ (although this is only important for calculating the Doppler boost factor η).

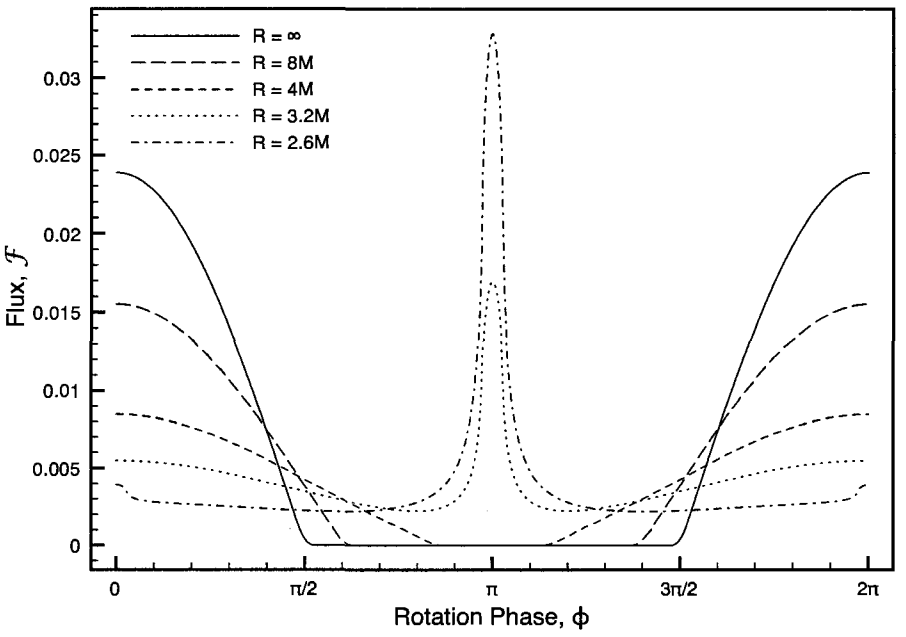

Figure 3.1: Light curves for of neutron stars of given radius with $\rho = 10°$, $i = \theta = 90°$, and $f(\alpha) = 1$. $R = \infty$ denotes the flat spacetime case.

3.1 Stellar Compactness

Figure 3.1 displays light curves for one revolution of a 10° diameter emitting spot with $i = \theta = 90°$ for stars of varying radius, as well as for a Newtonian or flat spacetime star represented by $R = \infty$ (compare to Figure 4 in Pechenick et al. [17]). The light curve in flat space goes to zero at $\phi = 95°$ as expected, while in the relativistic cases the effect of light bending is to keep the spot visible past $\phi = 95°$. As the radius decreases and gravity gets stronger the spot is visible longer, until at approximately $R = 3.52M$ the light bending becomes extreme enough that the spot is visible at all times, and a sharp peak in the light curve develops at $\phi = \pi$. This peak is caused by the gravitational lensing effect of the star on the spot itself at this point. Photons from the spot are bent around the star in all directions to reach the observer, forming a ring in his sky that can have total area greater than the spot itself even at $\phi = 0$. Since observed brightness is directly proportional to the area subtended in the observer's sky, we get the high peak in the light curve. As the radius decreases further to a point just above the photon sphere (about $R = 3.02M$), another, much smaller, peak forms at $\phi = 0$. This second peak is also produced by the gravitational lensing effect of the star. In this case, the light bending is so severe that photons emitted near $\phi = 0$ are able to circle the star

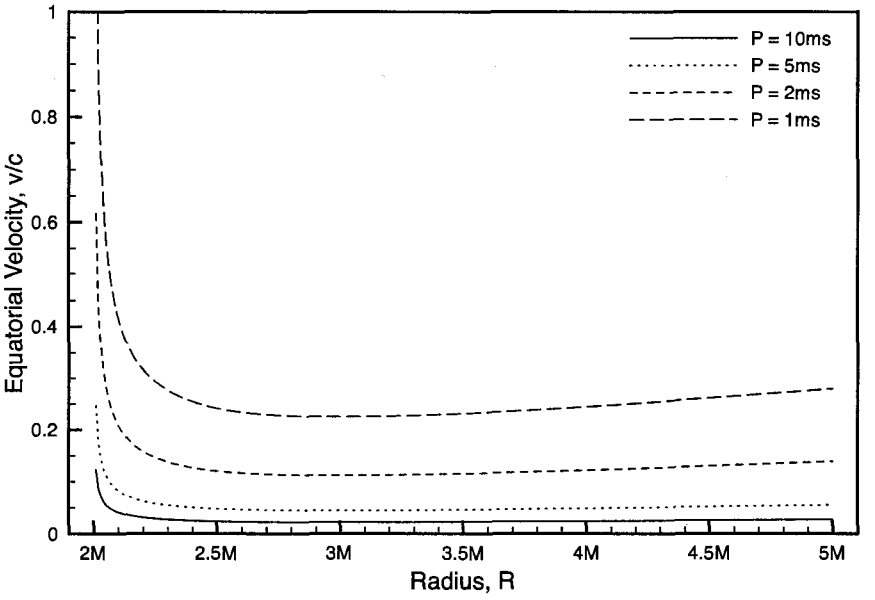

Figure 3.2: Equatorial velocity as a function of radius for neutron stars of mass $M = 1.4M_{\odot}$ and given observed rotation period P, calculated using the approximation of a Schwarzschild metric with corrections from special relativity. Note that the approximation fails very near the limit of $R = 2M$, but this is well below the finite pressure limit of $R = 2.25M$.

completely to come back around and still reach the observer, again forming a ring. When the radius falls below the photon sphere at $R = 3M$ and the star becomes ultracompact, not all of the light emitted by the spot can escape to reach the observer (we assume here that the light that falls back onto the star is not re-emitted). That which does, however, can still undergo the same severe light bending. The light curve of an ultracompact star, then, is almost entirely flat except for the two sharp peaks at $\phi = \pi$ and $\phi = 0$. In addition, as the radius of the star decreases, both peaks only grow more prominent over the remainder of the light curve. The ratio of their brightness to that of the continuum increases as the radius decreases. Likewise, the ratio of the amplitude of the larger peak to that of the smaller also increases as the radius of the star decreases.

3.2 Relativistic Doppler Shifts

In Figure 3.2 we have plotted equatorial velocity as a function of radius for several neutron stars with different observed rotation periods using our approximation of a

Schwarzschild metric with relativistic Doppler corrections. We can see that for stars above the finite pressure limit of $R = 2.25M$, the velocities involved only become highly relativistic (more than $0.1c$) for rotation periods on the order of 1-2 ms. Figure 3.3 compares the light curves produced by two revolutions of a 10° diameter spot with $i = \theta = 90°$ on neutron stars of radius $R = 3.2M$ with observed rotation periods of 1 s, 10 ms, and 1 ms. As Figure 3.2 suggests, only the 1 ms curve is significantly different; the 10 ms curve is almost identical to the 1 s one, which itself is indistinguishable from a curve with no Doppler corrections (not pictured). During the first half of a rotation, when the spot is moving away from the observer, the spot's emitted light is redshifted which results in a decrease in total flux detected by the observer. During the second half, the spot is moving toward the observer, resulting in the light being blueshifted and an increase in the detected flux. The most notable result of these relativistic Doppler shifts is that the 2 peaks in the light curve, which occur at $\phi = \pi$ and $\phi = 2\pi$ in the 1 s curve, have been increased in magnitude and moved into the blueshifted part of the curve. Notice also that at exactly $\phi = 2\pi$ the flux is reduced due to transverse Doppler redshifting, whereas at $\phi = \pi$ the lensed image has an increase in the overall flux of the image due to blueshifting. As a result the $\phi = \pi$ peak (which is caused by light bending) has been shifted to the right much less than the $\phi = 2\pi$ peak (which here is not caused by gravity) has been shifted to the left.

Figure 3.4 plots light curves for ultracompact neutron stars with the same properties as in Figure 3.3 except for radius. Examining all 4 graphs, we see that the differences between the 1 ms and 1 s curves diminish as the radius of the neutron star decreases; the effects of special relativity grow less significant as gravity becomes stronger. This is most evident in that blueshifting increases the magnitude of the $\phi = \pi$ peak less for smaller radius stars. There is another difference unique to the ultracompact star plots: the small $\phi = 2\pi$ peak actually decreases in magnitude due to Doppler shifting, unlike the peak in Figure 3.3, although it is moved very slightly into the blueshifted part of the curve. The reason for this discrepancy has to do with the multiple images produced by the star. At $\phi = 2\pi$ the primary image is dimmed as a result of transverse Doppler shifting but the secondary image is brightened in the same way as the $\phi = \pi$ peak above. These effects compete, with the dimming being stronger in the 1 ms curves, resulting in an overall decrease in flux for the $\phi = 2\pi$ peak. In fact, this sort of phenomenon takes place throughout the entire light curve. Since the secondary image is emitted in the opposite direction from the primary to loop around the star and reach the observer, it experiences the opposite Doppler shift: when the primary image is redshifted the secondary image is blueshifted and vice versa. This result serves to mitigate the Doppler shift effects

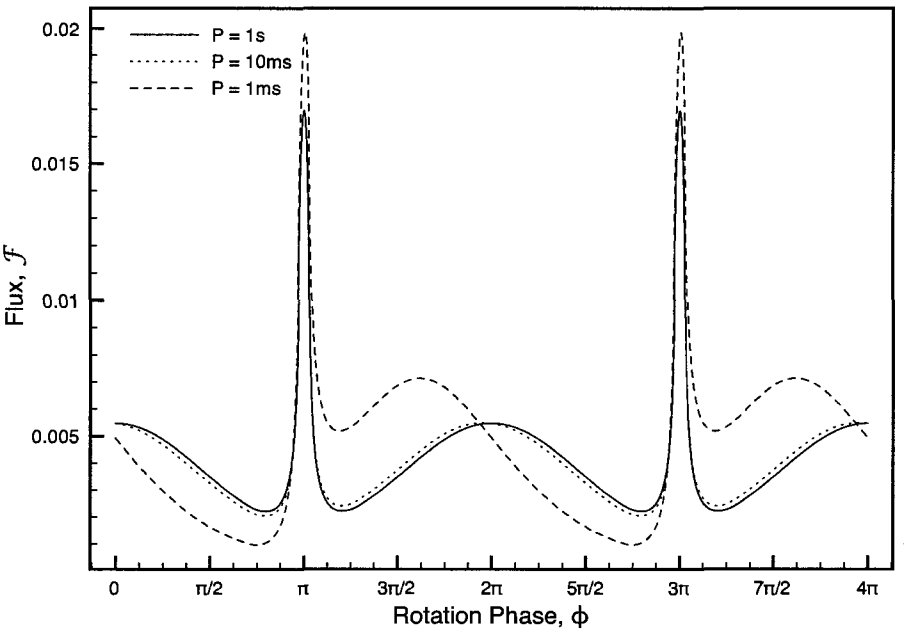

Figure 3.3: Light curves for neutron stars of radius $R = 3.2M$ with $\rho = 10°$, $i = \theta = 90°$, and $f(\alpha) = 1$ for given period P. Two full rotations are shown to better show the pulse shape near $\phi = 2\pi$.

described previously when multiple images are visible, and since the secondary image gets brighter relative to the primary as gravity increases, the overall Doppler effect grows weaker for more compact stars.

As a final comment, recall that our approximation for rotation fails to take into account such phenomena as frame dragging, oblateness of the star, the differing times of flight between photons emitted from different points on the star, and even the different times of arrival of the additional images. These effects tend to become significant under roughly the same conditions as our Doppler approximation, so from here on we will consider only configurations with a rotation period of 1 second, where the effects of rotation and special relativity are insignificant.

3.3 Spot Size

Figure 3.5 plots light curves from two revolutions of emitting spots of different angular diameter ρ with $i = \theta = 90°$ on stars of radius $R = 3.2M$. The majority of the curve varies as ρ^2 with the spot diameter — that is, it varies linearly with the area of the spot as expected — but the peak at $\phi = \pi$ exhibits different behaviour with respect to the size

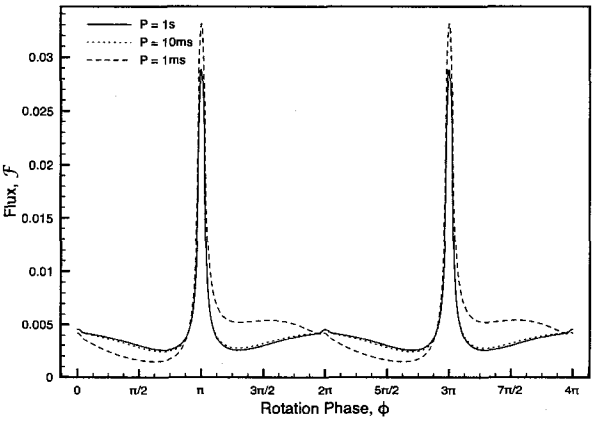

(a) R = 2.9M

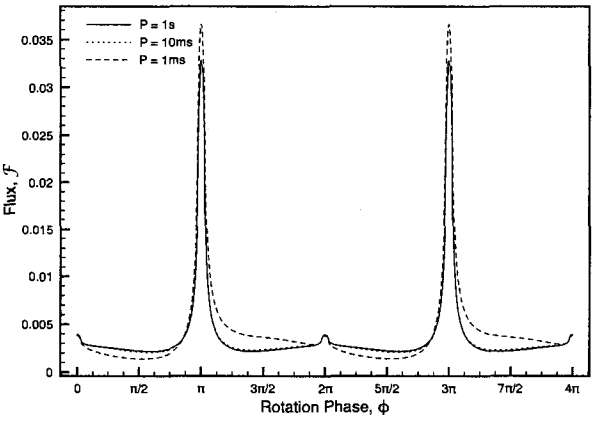

(b) R = 2.6M

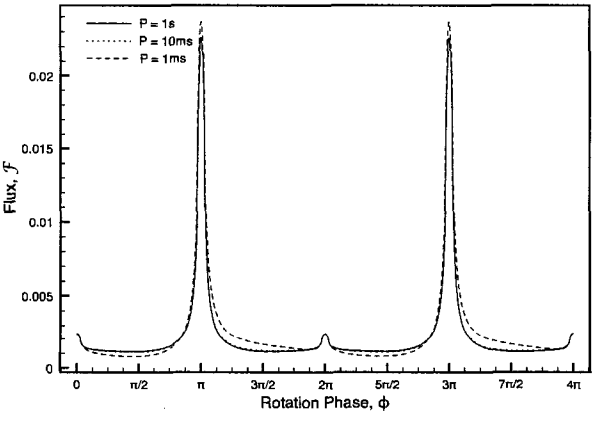

(c) R = 2.3M

Figure 3.4: Light curves for ultracompact neutron stars of given radius with $\rho = 10°$, $i = \theta = 90°$, and $f(\alpha) = 1$ for given period P.

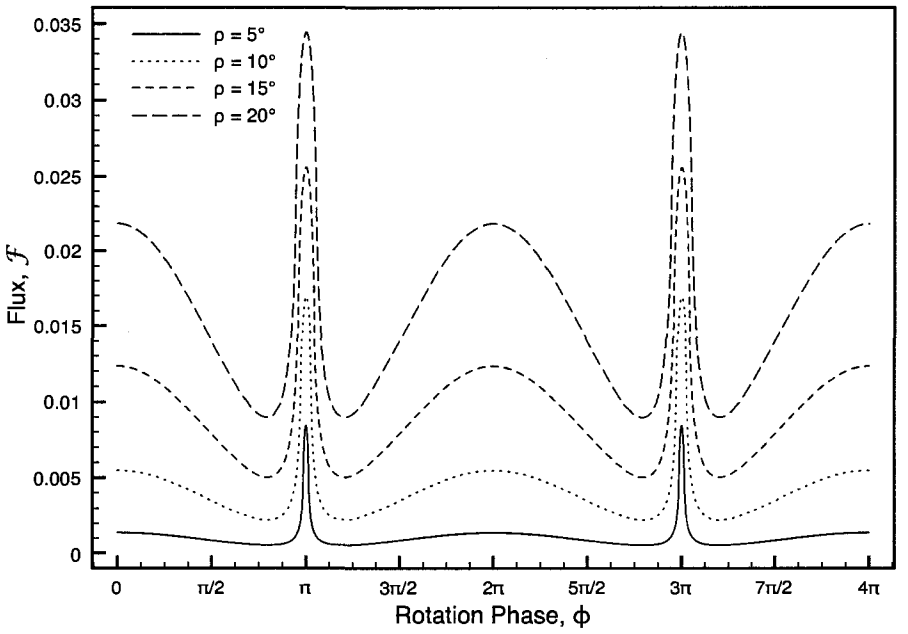

Figure 3.5: Light curves for neutron stars of radius $R = 3.2M$ with $i = \theta = 90°$ and $f(\alpha) = 1$ for given ρ.

of the spot. First of all, we observe that the width of the peak is similar to but slightly larger than the angular diameter of the spot. Second, as spot size increases the peak becomes less pronounced over the rest of the light curve. In fact, instead of increasing as ρ^2 like the rest of the curve, the amplitude of the peak varies very close to linearly with ρ. This result is best explained by the geometry of the image produced by the lensing. Recall that the brightness of an image is directly proportional to its area. Everywhere except at $\phi = \pi$, the observer sees one or more images of the spot, and while they may be distorted from the spot's original shape their area and therefore brightness increases directly with the area of the spot itself. At $\phi = \pi$, however, the observed image is a ring of light instead of one or more spots as discussed earlier. Here we expect that a larger value of ρ will only increase the thickness of the ring, and as described in Figure 3.6 the area of a thin ring increases with respect to its thickness in a linear fashion. Since the brightness of the peak is proportional to the area of the observed image at $\phi = \pi$, we thus expect it to vary linearly with ρ. In fact, the exact relation between the area of the ring and the size of the spot depends on the shape of the function $\psi(\alpha)$, but until the spot becomes very large the relation is approximately linear.

Figure 3.7 contains the same plots as Figure 3.5 except that they are for an ultracompact star of $R = 2.6M$. The behaviour of these curves and their relation to ρ is identical

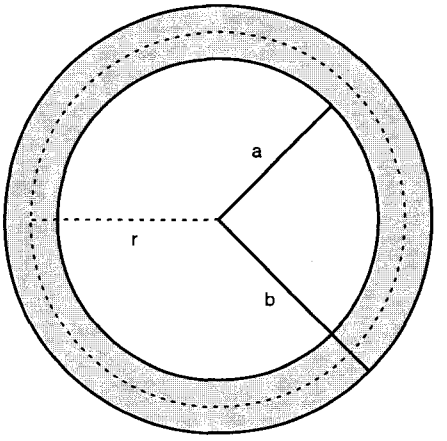

Figure 3.6: The area of the shaded ring is given by the formula $A = \pi\left(b^2 - a^2\right)$. Given expressions for the ring's thickness $c = b - a$ and its midpoint radius $r = (a + b)/2$, we can write the area formula as $A = 2\pi rc$. Differentiating this equation with respect to c gives us $\frac{\mathrm{d}A}{\mathrm{d}c} = 2\pi r + 2\pi c\frac{\mathrm{d}r}{\mathrm{d}c}$. If the ring is thin, i. e. $c \ll r$, then we can neglect the second term, with the result that the area of a thin ring depends linearly on its thickness.

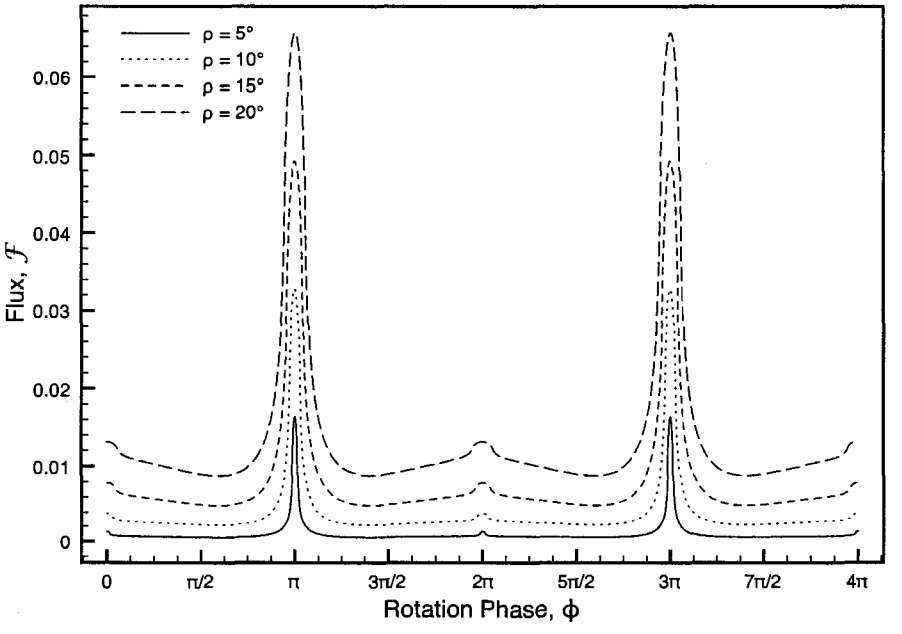

Figure 3.7: Light curves for neutron stars of radius $R = 2.6M$ with $i = \theta = 90°$ and $f(\alpha) = 1$ for given ρ.

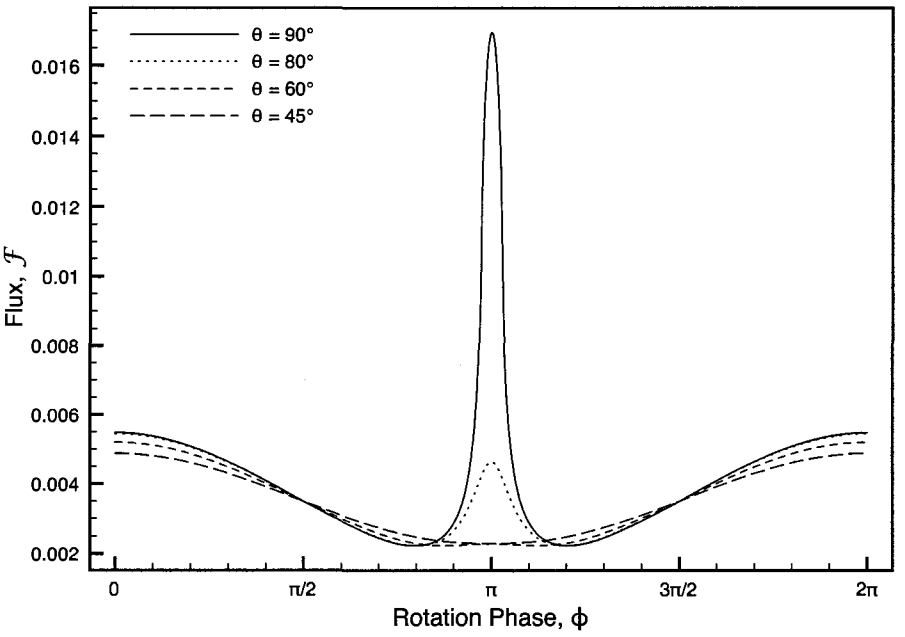

Figure 3.8: Light curves for neutron stars of radius $R = 3.2M$ with $\rho = 10°$, $i = 90°$. and $f(\alpha) = 1$ for given θ.

to that of the $R = 3.2M$ star everywhere except at the new peak at $\phi = 2\pi$. This peak has a width which is also similar to the diameter of the spot, but its amplitude varies with ρ in neither a strictly linear nor a strictly quadratic fashion. Instead, the relation best fits a polynomial equation of the form $a\rho^2 + b\rho$, where $b > a$. This form of relation arises because at $\phi = 2\pi$ the observer receives one primary image of the spot that varies as ρ^2, as well as a secondary gravitationally lensed image in the shape of a ring that varies as ρ (with the same caveat as before that the exact relation depends on $\psi(\alpha)$).

3.4 Spot Location

So far, all of our configurations have been for the special case $i = \theta = 90°$ where both the inclination angle and the emitting spot are at the equator of the star. Now we will examine more general cases where we allow one or both of these parameters to vary. In Figure 3.8 we plot one revolution of a 10° diameter emitting spot located at latitude θ with $i = 90°$ on a star of radius $R = 3.2M$. Since the peak at $\phi = \pi$ is a result of the spot being opposite the observer, it drops off rapidly as expected as the spot moves away from the equator; at $\theta = 80°$ the amplitude of the peak has dropped by over 80% from its amplitude given an equatorial spot. At $\theta = 60°$ its amplitude is less than 1%

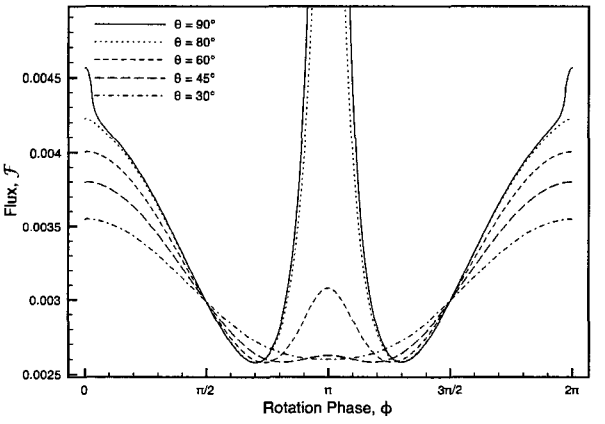

(a) R = 2.9M

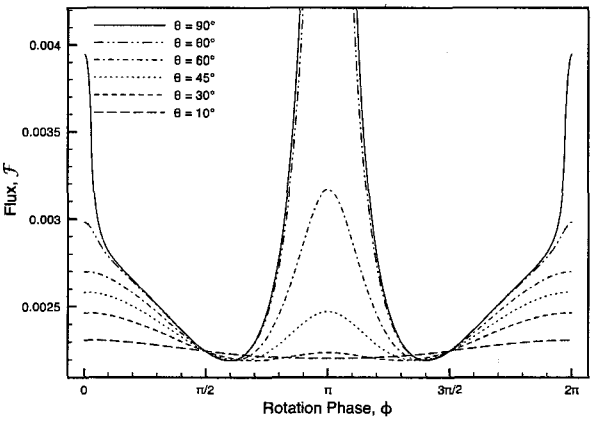

(b) R = 2.6M

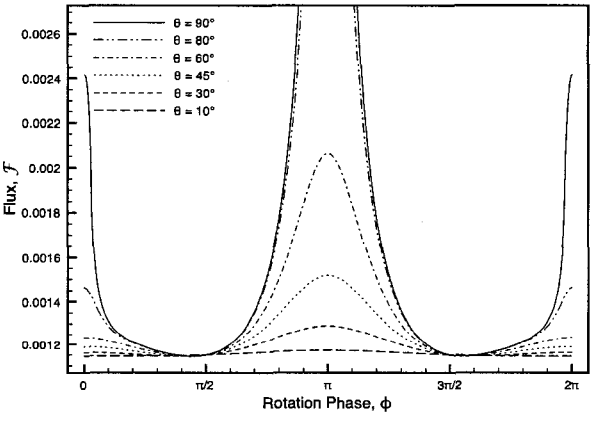

(c) R = 2.3M

Figure 3.9: Light curves for ultracompact neutron stars of given radius with $\rho = 10°$, $i = 90°$. and $f(\alpha) = 1$ for given θ.

of the maximum, and by $\theta = 50°$ the peak has disappeared completely, leaving nothing but a sine wave pattern that decreases in modulation for spots closer to the pole. We expect, then, that no more than 30-40% of all observers will observe a light curve with anything but a featureless sine wave pattern for this size neutron star. Figure 3.9 plots similar light curves for ultracompact stars. In these configurations there are two peaks to consider. The new peak at $\phi = 2\pi$ vanishes very quickly as we move the spot away from the equator; by $\theta = 80°$ it is at best barely noticeable and past that it has disappeared entirely. On the other hand, the behaviour of the peak at $\phi = \pi$ is qualitatively similar to the previous case. As the spot moves away from the equator, the amplitude of the peak drops rapidly, so that at $\theta = 80°$ it has been reduced by almost 80% from the maximum. We find, however, that as radius decreases the peak takes longer to become insignificant and disappear entirely. In the $R = 2.9M$ case, the peak doesn't vanish until about $\theta = 35°$; for $R = 2.6M$ the peak remains until approximately $\theta = 15°$; and in the most extreme case of $R = 2.3M$ the peak doesn't really vanish at all (discounting the trivial case of a spot located at the geographic pole). Regarding ultracompact stars, then, we expect that while no more than 10% of observers would see any feature at $\phi = 2\pi$, at least 60-65% of observers (more for non-causal stars) would see some peak at $\phi = \pi$, even for a single emitting spot.

In Figure 3.10 we take one revolution of a 10° diameter spot in the configuration $i = 180° - \theta$ for values of θ from 10° to 90°. In these cases, the emitting spot is always directly opposite the observer at $\phi = \pi$, so the amplitude of the peak is independent of θ; its width, on the other hand, increases as θ decreases. In addition, as θ decreases, the peak at $\phi = 0$ decreases and flattens out completely. Notice that the behaviour of the $\phi = \pi$ peak is identical in both the ultracompact case as well as the highly compact one. The $\phi = 0$ peak vanishes more quickly for the ultracompact case, but for low values of θ the two curves look qualitatively alike. Figure 3.11 follows one revolution of a 10° diameter spot in the configuration $i = \theta$, again for values of θ from 10° to 90°. Here, the emitting spot is always directly facing the observer at $\phi = 0$, so it is that peak whose amplitude is independent of θ, whereas the $\phi = \pi$ peak decreases and vanishes quickly as θ decreases. Unlike the previous configuration, however, here the light curves in the highly compact and ultracompact cases behave qualitatively different. In the case of the ultracompact $R = 2.6M$ star the width of the $\phi = 0$ peak increases as θ decreases, but the peak remains sharp and distinct even at $\theta = 10°$, whereas for the $R = 3.2M$ star the entire light curve flattens out as θ decreases and has a much smaller modulation at $\theta = 10°$.

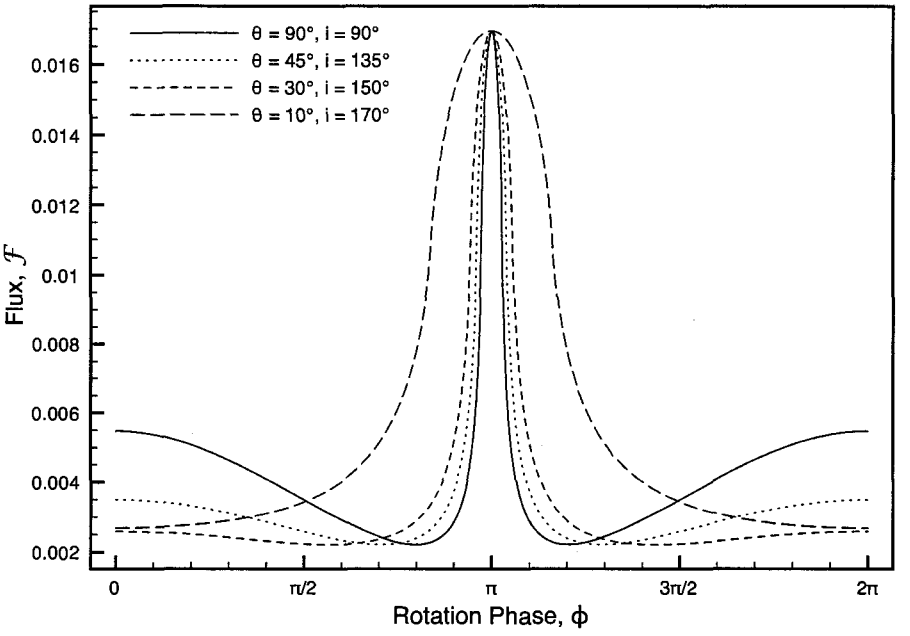

(a) R = 3.2M

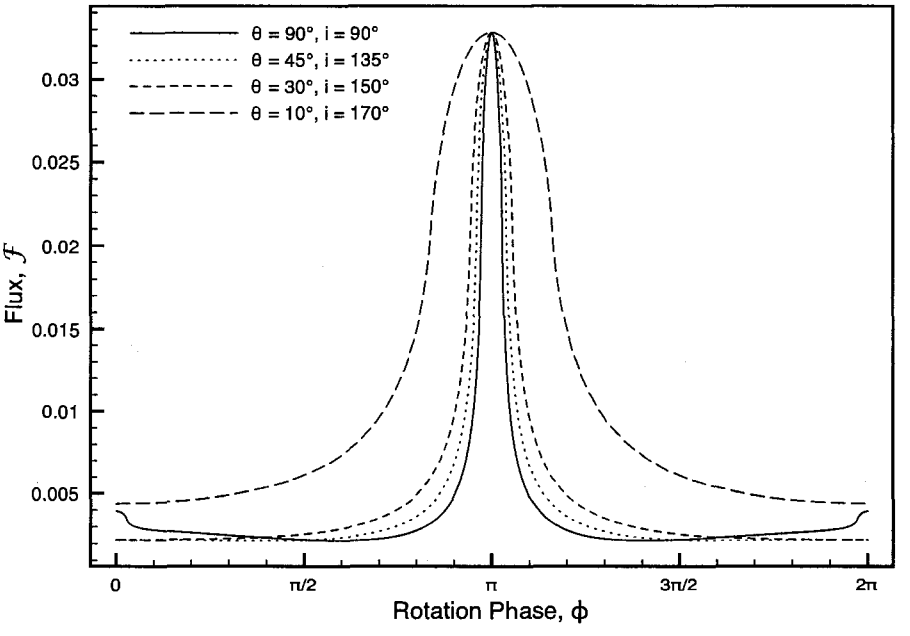

(b) R = 2.6M

Figure 3.10: Light curves for neutron stars of given radius with $\rho = 10°$ and $f(\alpha) = 1$ in the configuration $i = 180° - \theta$.

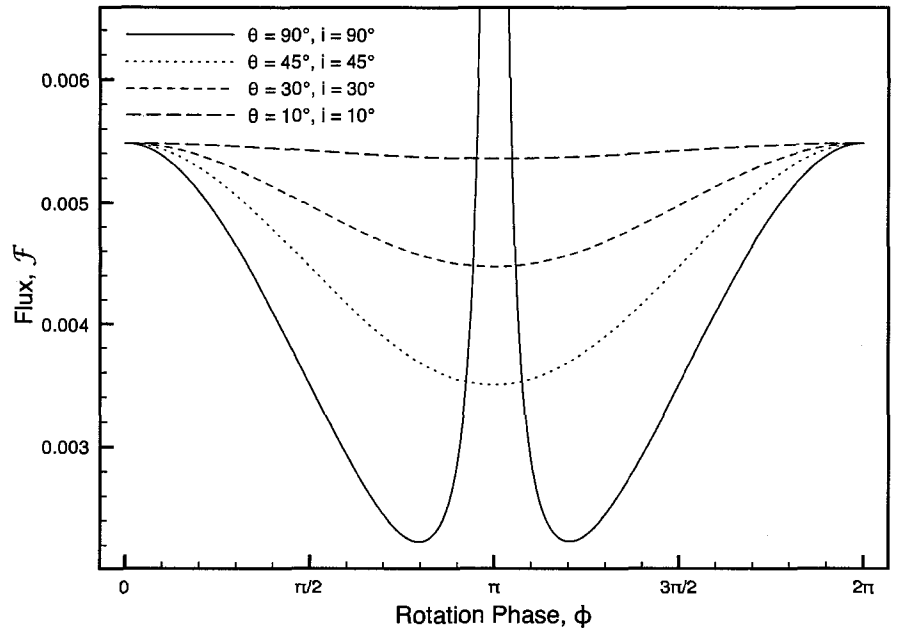

(a) R = 3.2M

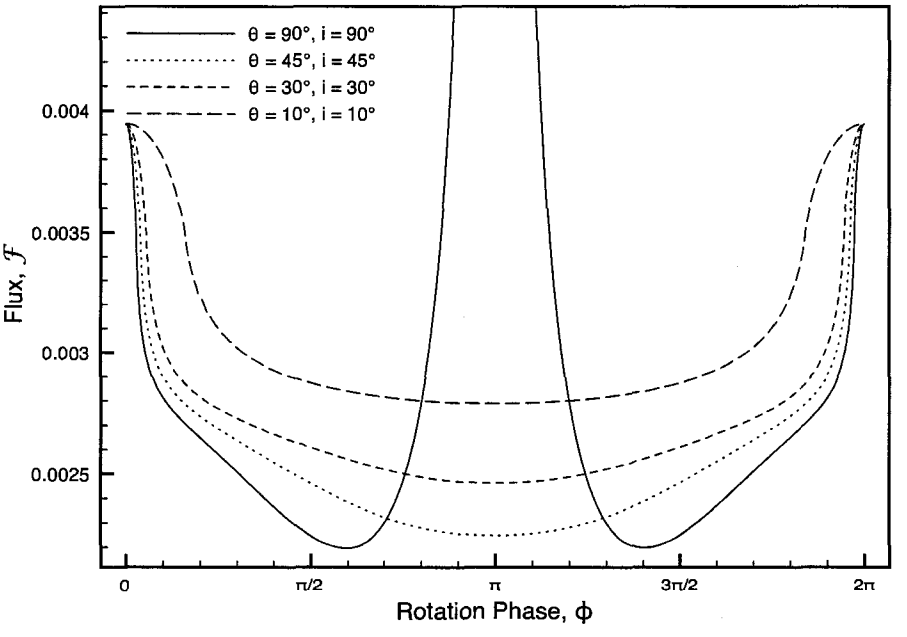

(b) R = 2.6M

Figure 3.11: Light curves for neutron stars of given radius with $\rho = 10°$ and $f(\alpha) = 1$ in the configuration $i = \theta$.

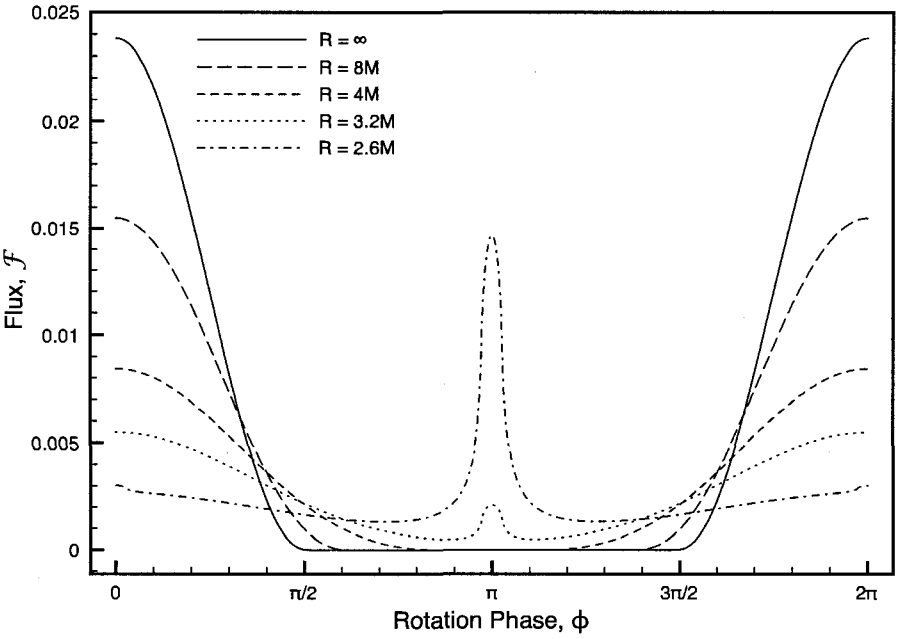

Figure 3.12: Light curves for neutron stars of given radius with $f(\alpha) = \cos\alpha$, $\rho = 10°$, and $i = \theta = 90°$. $R = \infty$ denotes the flat spacetime case.

3.5 Beamed Emission

Previously we have been restricting our investigation to isotropic emission from the star ($f(\alpha) = 1$), but now we also wish to examine a couple of cases of anisotropic or beamed emission. We begin with an example of focused beaming where photons emitted radially are preferred over those emitted tangent to the surface. In Figure 3.12 we plot the same graph as in Figure 3.1 except for taking $f(\alpha) = \cos\alpha$ (compare also to Figure 8 from Pechenick et al. [17]). For most stars, including highly compact ones, the effect of this type of beaming is to cause the observed flux from the star to drops off sooner and more quickly as it rotates from $\phi = 0$ compared to the isotropic case. In particular, for highly compact configurations the amplitude of the $\phi = \pi$ peak is significantly reduced (down to about 15% of its brightness when there is no beaming in the $R = 3.2M$ case) albeit not completely eliminated. With ultracompact stars, however, tangential photons cannot escape their gravity well to begin with, so although still present this effect is diminished. Furthermore, as radius decreases only the more radially emitted photons can reach the observer and so the beaming effect becomes less important. The peak at $\phi = \pi$ is still reduced compared to the case of isotropic emission but not as severely as for highly compact stars (for $R = 2.6M$ its amplitude falls only to about 50% of the

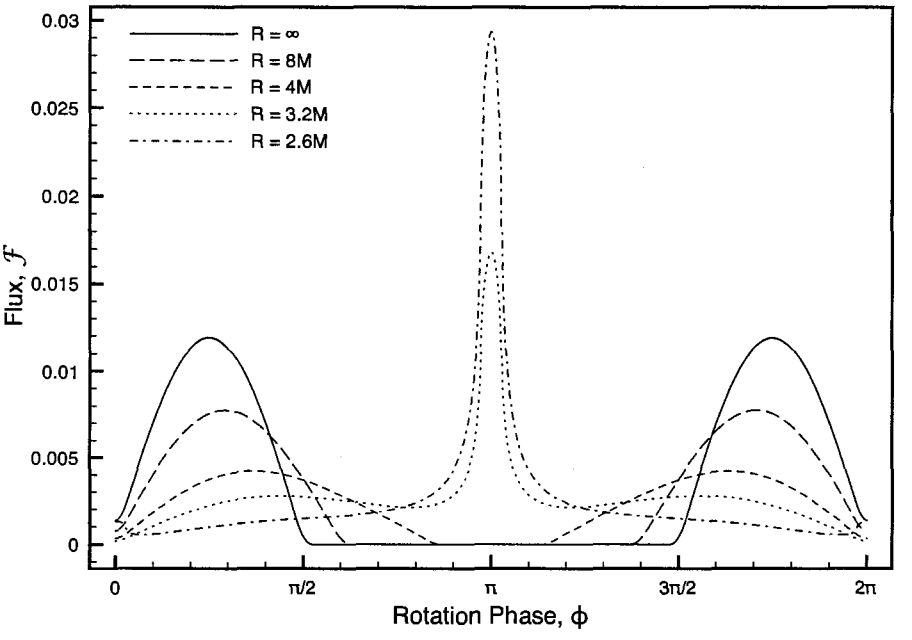

Figure 3.13: Light curves for neutron stars of given radius with $f(\alpha) = \sin\alpha$, $\rho = 10°$, and $i = \theta = 90°$. $R = \infty$ denotes the flat spacetime case.

value given isotropic emission). The much smaller $\phi = 0$ peak is reduced, too, to the point where it has mostly or completely vanished for $R \gtrsim 2.6M$.

The second case of anisotropic emission to consider is fanned beaming where tangentially emitted photons are preferred and radial photons suppressed. Figure 3.13 also plots a graph similar to Figure 3.1, but this time taking $f(\alpha) = \sin\alpha$ (again, compare to Figure 10 in Pechenick et al. [17]). Given this type of beaming, for all the stars except the ultracompact configurations the standard peak in the light curve at $\phi = 0$ is replaced by two smaller peaks at $\phi = \pm\pi/4$. The ultracompact stars, on the other hand, retain the secondary image and thus the peak at $\phi = 0$ even though the primary image disappears as it does for the larger stars. In addition, fanned beaming results in no diminishment of the $\phi = \pi$ peak for highly compact stars. Ultracompact stars see a small reduction in the brightness of that peak since the tangential photons prefered by the beaming fall back onto the star's surface. Even so, the most extreme case of $R = 2.3M$ only sees the peak's amplitude reduced to 70% of its value given no beaming. The peaks in the light curve that are due to gravitational lensing are barely changed by fanned beaming, whereas they are greatly reduced by focused beaming.

3.6 Discussion

From previously in this chapter, we have seen that the primary distinguishing feature of light curves from highly compact and ultracompact neutron stars is the sharp peak that is seen when the emitting spot is opposite to the observer. Depending on the size of the spot and of the star itself, this peak can be upwards of 5-10 times as bright as any other part of the light curve. Of course, while identifying the unique and distinguishing features of these types of neutron stars is useful, it is also important to determine if and when these features disappear and we observe mundane light curves. Typically, observed pulsars that show no signs of eclipsing produce light curves in the shape of fairly unremarkable sine wave patterns with low modulation. For example, the pulsations from the neutron star SAX J1808 take the form of a sine wave with roughly 10% modulation [18]. Recent work to match the observed curve to a theoretical model of the star have neglected the possibility of multiple images due to the increased computational difficulty in taking them into account and the assumption that multiple images are unlikely to produce such curves [12, 18] (notably, though, both of these papers present one possible best fit model that is a highly compact star where the emitting spot never enters the multiply imaged region). Thus we wish to find out under what circumstances if any can a highly compact or ultracompact star produce such a light curve, particularly if we require that the emitting spot be multiply imaged.

The key our investigations is found in Section 3.4, where we looked at the light curves for neutron stars with $i = 90°$ and varying θ. For highly compact stars that have both a singly imaged region and a multiply imaged region, one might assume that if the emitting spot enters the multiply imaged region the light curve has a peak at $\phi = \pi$ and otherwise it is a featureless sine wave. While this relation roughly holds for stars with a small multiply imaged region (those with $R/M \gtrsim 3.2$), in more compact stars it does not. In addition, ultracompact stars where the spot is always multiply imaged can produce light curves that are simple sine waves. As an example, let us return to SAX J1808 whose light curve is a sine wave with modulation of roughly 10%. Taking the parameters $R = 3.2M$, $i = 90°$, and $\theta = 10°$ gives us a sine wave with 10% modulation, but here the emitting spot never enters the multiply imaged region. On the other hand, given $R = 2.9M$, $i = 90°$, and $\theta = 20°$ also produces a sine wave with about 10% modulation, but here the star is ultracompact and the spot is always multiply imaged. We must conclude that the assumption that a multiply imaged spot is unlikely to produce this shape of light curve is false and that such models should not necessarily be neglected from analysis.

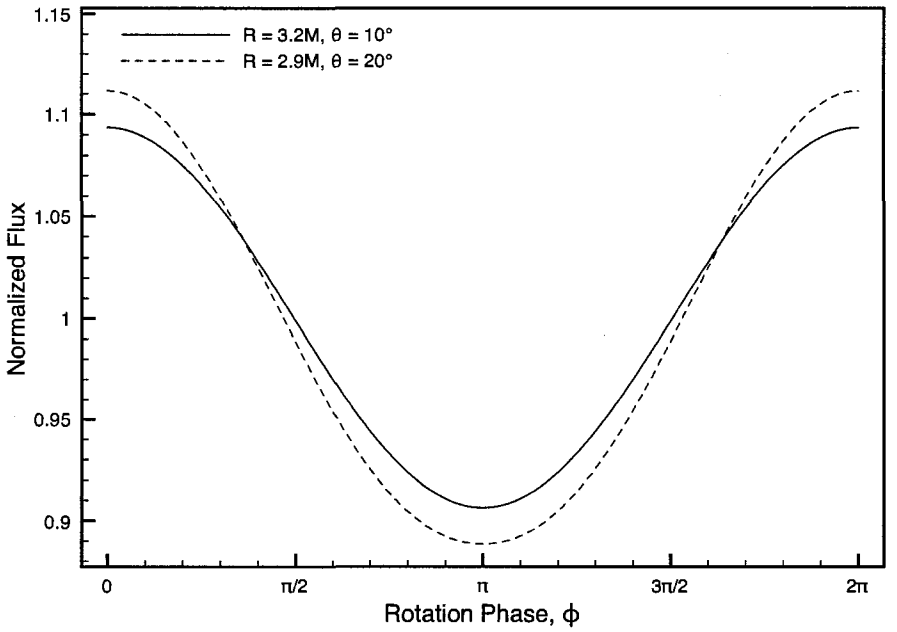

Figure 3.14: Light curves for a highly compact and an ultracompact neutron star showing a sine wave pattern with approximately 10% modulation. For both cases $\rho = 10°$ and $i = 90°$.

R/M	3.5	3.4	3.3	3.2	3.1	3.0	
ϑ	170°	160°	152°	143°	137°	132°	
R/M	2.9	2.8	2.7	2.6	2.5	2.4	2.3
ϑ	126°	120°	114°	107°	99°	90°	79°

Figure 3.15: Table of ϑ as a function of neutron star compactness R/M.

To explain this behaviour in the more general case where we allow i to vary, recall that for a highly compact or ultracompact neutron star when $i+\theta = 180°$ the spot passes a point directly opposite the observer at $\phi = \pi$, producing the huge distinguishing peak in the light curve. In order to eliminate that peak completely the spot must not pass anywhere near there, meaning we must have $i + \theta < \vartheta$, where ϑ is a function of the star's compactness R/M. An empirically determined table of values for this function is provided in Figure 3.15. Recall also that when $i - \theta = 0°$ stars with $R/M < 3.02$ have a much smaller peak in the light curve at $\phi = 0$ when the spot passes directly in front of the observer. For these stars to produce a light curve that is a featureless sine wave we require that in addition to the above $i - \theta \gtrsim 15°$.

Chapter 4

Conclusion

4.1 Summary of Completed Research

The study of what we call highly compact and ultracompact neutron stars is an area that has not been explored in great detail. The extreme gravity of the highly compact stars creates an added level of complexity, as certain regions of the star can produce multiple images that are all visible to the same observer. With the ultracompact stars not only is the entire surface of the star multiply imaged but some of the light emitted from the star cannot escape its powerful gravity and falls back in on it. In this thesis, we developed a procedure and computer code to incorporate these effects and numerically calculate the light curves that a distant observer would see from a hot spot on a very compact neutron star.

With our method in place, we produced light curves for many different configurations of very compact stars to determine their distinguishing features and under what circumstances they are and are not observable. We first looked at how increasing the star's gravity changed the light curve, and found that it flattened out and developed first one sharp, very bright peak and then another smaller one as we got to very compact stars. To follow up, we investigated what effect Doppler shifts from rapid rotation had on the light curve, and how it depended on the size of the emitting spot. Then we discovered that the presence and strength of the peaks in the curve was determined by the location of the spot on the star and the star's orientation with respect to the observer. Finally we examined how the peaks were affected by anisotropic emission from the star and saw that while fanned beaming had little effect on them, focussed beaming reduced their amplitude significantly.

The last thing that we did was compare some of our data to some observed pulsations

from the neutron star SAX J1808. We noticed that previous attempts to match the observed light curve from the star had neglected the possibility of the emitting spot being multiply imaged. The observed light curves from SAX J1808 were in the shape of sine waves with low (~10%) modulation, and it was assumed that stars where the emitting spot was multiply imaged would not easily produce those shape of curve. However, we were able to produce featureless sine wave patterns of the required modulation even when the spot was in a multiply imaged region of the star for part or all of a rotation, and even when the star was ultracompact.

4.2 Directions for Future Research

There are a few avenues of inquiry that we did not go down in this work. First of all, one can extend examination of the light curves by considering different forms of the beaming function, or by looking into a more accurate treatment of rapidly rotating stars since our approximation of such neglected several factors. Particularly interesting would be to incorporate photon times of arrival, since for a multiply imaged spot the different images will take different amounts of time to reach the observer. Perhaps more notable, though, is that here we only looked at the case of a single emitting spot on the star. It is also common, however, for a neutron star to have two antipodal hot spots, when light is emitted in a two beams aligned with both thenorth and south magnetic poles, for example. Fortunately, calculating the observed flux for antipodal spots is very simple: If the flux from a single spot located at (θ_c, ϕ_c) is given by $\mathcal{F}$ as described in Section 2.3, then the two spot flux is given by $\mathcal{F}_2(\theta_c, \phi_c) = \mathcal{F}(\theta_c, \phi_c) + \mathcal{F}(\pi - \theta_c, \pi + \phi_c)$. The shape of the two spot light curve and how the various parameters such as spin, spot size and location, and beaming affect it should be straightforward to do, but it is left for future work.

In Section 3.6, we concluded that neglecting the possibility of stars with multiply imaged spots when trying to model observed light curves is not necessarily a good assumption. It is very possible for such stars to produce light curves that match up qualitatively to observations. It is a good idea, then, to go back and find out if these stars can produce a best fit model for observed pulsations from neutron stars like SAX J1808, or if they can be eliminated from consideration for other reasons.

Bibliography

[1] Beloborodov, A. M., 2002, Astrophys. J. **566**, L85.

[2] Bildsten, L., and T. Strohmayer, 1999, Phys. Today. **52**, 40.

[3] Cadeau, C., D. A. Leahy, and S. M. Morsink, 2005, Astrophys. J. **618**, 451.

[4] Cadeau, C., S. M. Morsink, D. Leahy, and S. S. Campbell, 2007, Astrophys. J. **654**, 458.

[5] Cook, G. B., S. L. Shapiro, and S. A. Teukolsky, 1994, Astrophys. J. **424**, 823.

[6] Ftaclas, C., M. W. Kearney, and K. Pechenick, 1986, Astrophys. J. **300**, 203.

[7] Haensel, P., J. P. Lasota, and J. L. Zdunik, 1999, Astron. Astrophys. **344**, 151.

[8] Hartle, J. B., 2003, *Gravity: An Introduction to Einstein's General Relativity* (Addison Wesley).

[9] Hessels, J. W. T., S. M. Ransom, I. H. Stairs, P. C. C. Freire, V. M. Kaspi, and F. Camilo, 2006, Science. **311**, 1901.

[10] Iyer, B. R., C. V. Vishveshwara, and S. V. Dhurandhar, 1985, Class. Quantum Grav. **2**, 219.

[11] Lattimer, J. M., and M. Prakash, 2007, Phys. Rep. **442**, 109.

[12] Leahy, D. A., S. M. Morsink, and C. Cadeau, 2008, Astrophys. J. **672**, 1119.

[13] Lindblom, L., 1984, Astrophys. J. **278**, 364.

[14] Misner, C. W., K. S. Thorne, and J. A. Wheeler, 1973, *Gravitation* (W. H. Freeman and Company).

[15] Negi, P. S., and M. C. Durgapal, 1999, Gen. Rel. Grav. **31**, 13.

[16] Nemiroff, R. J., P. A. Becker, and K. S. Wood, 1993, Astrophys. J. **406**, 590.

[17] Pechenick, K. R., C. Ftaclas, and J. M. Cohen, 1983, Astrophys. J. **274**, 846.

[18] Poutanen, J., and M. Gerliński, 2003, Mon. Not. R. Astron. Soc. **343**, 1301.

[19] Press, W. H., S. A. Teukolsky, W. T. Vetterling, and B. P. Flannery, 1988, *Numerical Recipes in C: The Art of Scientific Computing* (Cambridge University Press), second edition.

[20] Rindler, W., 1982, *Introduction to Special Relativity* (Oxford University Press), second edition.

[21] Schwarzschild, K., 1916, Sitzungsber. Preuss. Akad. Wiss. Berlin, Phys.-Math. Klasse, 189. Translation available at physics/9912033.

[22] Shapiro, S. L., and S. A. Teukolsky, 1983, *Black Holes, White Dwarfs, and Neutron Stars* (John Wiley & Sons, Inc.).

[23] Wijnands, R., and M. van der Klis, 1998, Astrophys. J. **507**, L63.